Journal of Applied Physics

Prediction of room-temperature multiferroicity in strained $MoCr_2S_6$ monolayer

Cite as: J. Appl. Phys. **127**, 155302 (2020); https://doi.org/10.1063/1.5144535
Submitted: 07 January 2020 . Accepted: 01 April 2020 . Published Online: 15 April 2020

Li-Zhe Liu, Kyung-Hwan Jin, and Feng Liu

Journal of Applied Physics ARTICLE scitation.org/journal/jap

Prediction of room-temperature multiferroicity in strained $MoCr_2S_6$ monolayer

Cite as: J. Appl. Phys. **127**, 155302 (2020); doi: 10.1063/1.5144535
Submitted: 7 January 2020 · Accepted: 1 April 2020 ·
Published Online: 15 April 2020

Li-Zhe Liu,[1,2,a)] Kyung-Hwan Jin,[2] and Feng Liu[2,a)]

AFFILIATIONS

[1]Collaborative Innovation Center of Advanced Microstructures, National Laboratory of Solid State Microstructures, Nanjing University, Nanjing 210093, People's Republic of China
[2]Department of Materials Science and Engineering, University of Utah, Salt Lake City, Utah 84112, USA

Note: This paper is part of the Special Topic on Beyond Graphene: Low Symmetry and Anisotropic 2D Materials.
[a)]**Authors to whom correspondence should be addressed:** lzliu@nju.edu.cn and fliu@eng.utah.edu

ABSTRACT

The contrasting *d*-orbital occupation required for ferroelectricity vs ferromagnetism makes it difficult for their coexistence in two-dimensional materials, especially at high temperature. To resolve this intrinsic contradiction, we propose a layered $MoCr_2S_6$ multiferroics by alloying magnetic Cr element into the ferroelectric 1T phase of the MoS_2 matrix. First-principles calculations disclose that a spontaneous symmetry breaking, depending on the Mo atom displacement, leads to a robust ferroelectricity, which coexists with a ferromagnetic order originated from two neighboring Cr atoms. The effect can be further enhanced by tensile strain to bring about a room-temperature multiferroicity. Our findings shed new light on the fundamental understanding of multiferroics and display promising applications in spintronics and multistate data storage.

I. INTRODUCTION

Two-dimensional (2D) materials that simultaneously possess ferroelectricity and ferromagnetism, especially at room temperature, have attracted much attention because of their potential applications in the next generation of spintronics and memory devices.[1–5] However, the coexistence of robust ferromagnetic and ferroelectric order in one 2D material is very rare, because of the inherent exclusion between ferroelectricity and ferromagnetism. Ferroelectrics are typically semiconductors that exhibit a spontaneous ferroelectric polarization arising from symmetry breaking, which requires off-center cations with empty or fully occupied 3*d*-orbitals.[6,7] In contrast, ferromagnetism typically originates from partially filled 3*d*-orbitals, whose strong *d*–*d* Coulomb interaction suppresses the appearance of spontaneous ferroelectric dipoles. To overcome this intrinsic contradiction in 3*d*-orbital occupation, we propose an alloying strategy to design a 2D material consisting of two different cations: one with the fully occupied 3*d*-orbitals moving to off-center positions away from the centrosymmetric sites to induce ferroelectric polarization, whereas the other has unpaired 3*d* electrons providing the necessary magnetic order. Furthermore, a room-temperature multiferroicity is shown to be attainable by applying tensile strain.

In order to realize multiferroicity, first, the candidate materials must be ferromagnetic semiconductors. This has inspired us to search for the possibility of combining the reported 2D ferroelectric materials (e.g., 1T MoS_2, functionalized graphene, SnSe, and phosphorene[8–12]) with the ferromagnetic materials (e.g., $Cr_2Ge_2Te_6$ and CrI_3[13,14]). We have chosen the ferroelectric (1T MoS_2) and ferromagnetic (CrI_3) combination as a candidate. We recognized that the Cr element is a good magnetic source that belongs to the same main group as Mo so that a Mo–Cr alloy may lead to coexistence of ferromagnetism and ferroelectricity. Through structural screening of a series of trials, such as $Mo_1V_2S_6$, $Mo_2V_1S_6$, $Mo_1Cr_2S_6$, $Mo_2Cr_1S_6$, $Mo_1Mn_2S_6$, $Mo_2Mn_1S_6$, $Mo_1Fe_2S_6$, $Mo_2Fe_1S_6$, $Mo_1Co_2S_6$, $Mo_2Co_1S_6$, $Mo_1Ni_2S_6$, and $Mo_2Ni_1S_6$ (see Table I), we discover that spontaneous symmetry breaking induced by the displacement of the Mo atom in the $MoCr_2S_6$ monolayer, accompanied with a metal–semiconductor transition, brings about a robust ferroelectric polarization. At the same time, the two nearest-neighbor Cr atoms can form a stable ferromagnetic configuration with a Curie temperature of approximately 145 K (higher than that of CrI_3 and $Cr_2Ge_2Te_6$).[13,14] Furthermore, structural deformation induced by strain in $MoCr_2S_6$ will partly suppress the ferroelectric

TABLE I. Electronic structure and magnetism in different alloys.

Type	Magnetism	ΔE (meV)	Moment (μ_B)	Property	Bandgap (eV)
MoS_2	Nonmagnetic	…	…	Semiconductor	0.78
$Mo_1V_2S_6$	AFM	−80.1	1.02	Half-metal	…
$Mo_2V_2S_6$	AFM	−35,7	0.98	Half-metal	…
$Mo_1Cr_2S_6$	FM	22.6	2.98	Semiconductor	0.32
$Mo_2Cr_1S_6$	FM	5.3	2.87	Metal	…
$Mo_1Mn_2S_6$	AFM	−8.8	3.93	Metal	…
$Mo_2Mn_1S_6$	AFM	−4.1	1.94	Metal	…
$Mo_1Fe_2S_6$	FM	17.8	2.02	Semiconductor	0.25
$Mo_2Fe_1S_6$	AFM	−20.9	1.98	Semiconductor	0.07
$Mo_1Co_2S_6$	Nonmagnetic	…	0.00	Metal	…
$Mo_2Co_1S_6$	Nonmagnetic	…	0.00	Semiconductor	0.06
$Mo_1Ni_2S_6$	Nonmagnetic	…	0.00	Semiconductor	0.28
$Mo_2Ni_1S_6$	Nonmagnetic	…	0.00	Semiconductor	0.18

polarization but can effectively enhance the Curie temperature to 300 K, realizing a room-temperature multiferroicity.

II. COMPUTATIONAL DETAILS

The first-principles calculations are based on density functional theory (DFT) as implemented in the Vienna *ab initio* simulations package (VASP),[15] with the Perdew–Burke–Ernzerhof (PBE) functional in the scheme of the generalized gradient approximation (GGA).[16] The Monkhorst–Pack *k*-points grid used is $9 \times 9 \times 1$ and the plane-wave cutoff energy is set to be 480 eV. Structural relaxation is carried out until all atomic forces are converged to be 0.01 eV/Å, and the vacuum space is adopted to be 20 Å, which was tested to be well converged. For Cr, we tested different U (1–4 eV) for the DFT + U calculations (see Fig. S1 in the supplementary material), and we found that all U values give qualitative the same results while $U = 3$ eV gives the best agreement with the previous report in a related system.[17] The ferroelectric polarization was calculated using the Berry phase methods.[18]

III. RESULTS AND DISCUSSION

Specifically, to harvest ferromagnetism and ferroelectricity simultaneously in a $MoCr_2S_6$ alloy, a $\sqrt{3} \times \sqrt{3}$ supercell was constructed. This choice was made because T phase MoS_2 with a (1×1) primitive is unstable, which spontaneously transforms into a more stable configuration with a $\sqrt{3} \times \sqrt{3}$ supercell.[8] The $MoCr_2S_6$ monolayer with centrosymmetric (named T) structure, as shown in Fig. 1(a), is found in a nonpolar ferromagnetic metal [see the band structure in Fig. 2(a)]. The calculated phonon dispersion of the T structure exhibits some unstable modes [see Fig. 2(b)], due to the tendency of spontaneous Mo displacement in the plane of $MoCr_2S_6$ [along the marked red arrow in Fig. 1(a)]. As expected, a Mo distortion in the T structure causes symmetry breaking and ferroelectric polarization, leading to an energy reduction of 0.14 eV/cell compared to the T structure [see Fig. 1(e)]. The lowest imaginary phonon of $MoCr_2S_3$ is also located near the K point. Trimerization of Mo is consistent with the previous reports.[19,20] It involves predominantly Mo displacement in the plane of the $MoCr_2S_6$ monolayer that would lead to Mo trimerization analogous to dimerization arising from a Peierls instability in one dimension.[8] In addition, the potential energy barriers of the antisymmetric displacement in Fig. S2 in the supplementary material disclose that the structural transition from T to Td phase is more favorable. The two neighboring Mo–S3 and Mo–S5 bonds are asymmetrically deformed, resulting in unbalanced charges in Fig. 1(b), but the Cr–S bonds remain unchanged. More importantly, upon the structural transformation from the T to noncentrosymmetric (named Td) phase, a gap of 0.32 eV opens in the band structure [Fig. 1(c)], leading to a metal-to-semiconductor transition. In addition, the typical spin-polarization originating from the Cr atom makes it to become a magnetic semiconductor. From the difference in the charge density plot of T and Td structure [Fig. 1(d)], one sees that some electrons are transferred to sulfur atoms to induce a charge separation (marked by "+" and "–"). This indicates that the Td structure with a noncentrosymmetric polarity results in a ferroelectric polarization.

Figure 1(f) illustrates the fundamental physical mechanism underlying the ferroelectricity. It is generally known that ferroelectric polarization is generated by the separation between positive and negative charges, for which the candidate structures should possess a stable Td symmetry [bottom panel in Fig. 1(b)] and be semiconducting in nature. However, the T phase gives rise to a nonpolar uniform charge distribution in a perfect 2D hexagonal lattice [upper panel in Fig. 1(b)]. On the other hand, ferromagnetism originates from partial occupation of the 3*d*-orbital of magnetic cation. As shown in Fig. 1(e), the Td structure will easily transform into the T structure, resulting in disappearance of ferroelectricity. Specifically, as shown in Fig. 1(f), the strong *d*–*d* Coulomb interaction between transition metal elements splits the chromium–sulfur (Cr–S)* antibonding band into one empty upper-Hubbard band (UHB) and one filled lower-Hubbard band (LHB).[21,22] When the energy difference between (Cr–S) bonding state and (Cr–S)* antibonding state, i.e., the charge transfer energy Δ is larger than U value (i.e., $\Delta > U$), the *d*-electron in LHB becomes delocalized hybridizing with nearby anions, to reduce the *d*-orbital occupation. Consequently, the Td structure becomes more stable. For $U > \Delta$, the *d*–*d* Coulomb interaction drives the LHB into

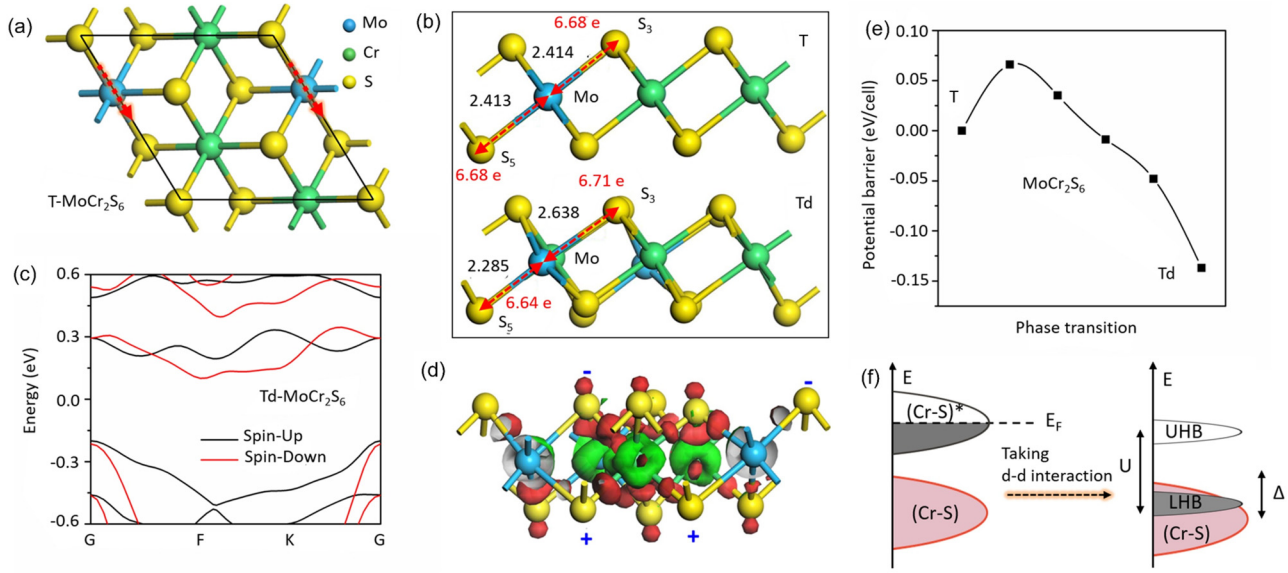

FIG. 1. (a) Displacement vectors (red arrows) of the Td phase with respect to the T phase. (b) The structural distortion from T- to Td-$MoCr_2S_6$ with a $\sqrt{3} \times \sqrt{3}$ supercell. (c) The band structure of the Td-$MoCr_2S_6$ monolayer. (d) An isosurface of the difference in charge densities between Td and T phases. (e) The structural transition between T and Td phase. (f) Schematic energy bands in consideration of Mott–Hubbard splitting.

the (Cr–S) bonding band, resulting in a preferred centrosymmetric T structure due to the inertness of *d*-electron in the LHB "protected" by Cr–S band.[21,22]

This structural transition is further confirmed by the calculated energy difference between T and Td structure using the DFT + U (U = 1–4 eV) method (see Fig. S3 in the supplementary material), indicating its structural stability. Figure 3(a) shows that the phonon dispersion of the Td phase does not display any imaginary frequency (energy < 0), indicating its dynamic stability. To further explore the structural stability, the $(2 \times 2 \times 1)$ $MoCr_2S_6$ supercell is calculated by *ab initio* molecular dynamics simulation with Nose–Hoover thermostat at 300 K. Figure 3(b) shows the fluctuation in the temperature as a function of simulation time at 300 K. Through 3.5 ps, the unstable T phase can spontaneously transform into the Td phase at room temperature, as shown in Figs. 3(c) and 3(d). Additionally, formation energies of randomly distributed Mo–Cr alloy are higher than that of ordered $MoCr_2S_6$ (Fig. S4 in the supplementary material). These calculations suggest the experimental feasibility of realizing ferroelectric polarization in $MoCr_2S_6$.

To obtain the Curie temperature, we also performed Monte Carlo (MC) simulations using a $12 \times 12 \times 1$ matrix, which is based on the classical spin Hamiltonian: $H = J_1 \sum_{\langle i,j \rangle} \boldsymbol{S}_i \cdot \boldsymbol{S}_j + J_2 \sum_{\ll i,j \gg} \boldsymbol{S}_i \cdot \boldsymbol{S}_j + J_3 \sum_{i,j} \boldsymbol{S}_i \cdot \boldsymbol{S}_j + D \sum_{\langle i \rangle} \boldsymbol{S}_{i,x0}^2$, where $\boldsymbol{S}_i$ and $\boldsymbol{S}_j$ are the net spin; J_1, J_2, and J_3 represent the first-, second-, and third-nearest magnetic coupling strength.[3,23] $S_{i,x0}$ and D represent the component of S_i along the in-plane easy-axis direction and the single-ion anisotropy parameter, respectively. The Metropolis method is adopted in our simulations.[24] When the system reaches equilibrium at a given temperature, the specific heat can by

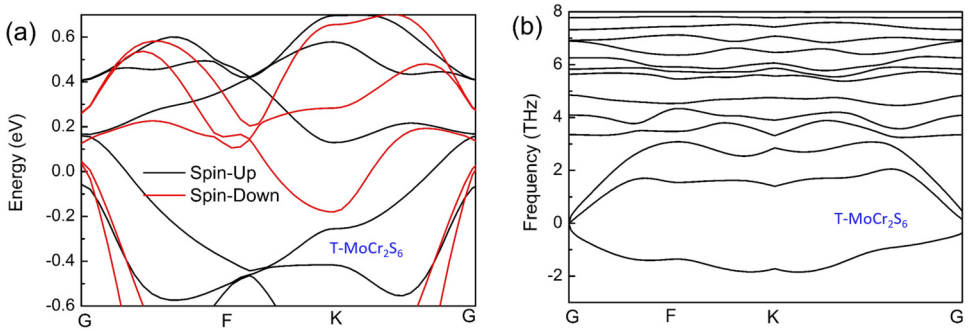

FIG. 2. (a) The calculated band structure of the T-$MoCr_2S_6$ monolayer. (b) The calculated phonon dispersion of the T-$MoCr_2S_6$ monolayer.

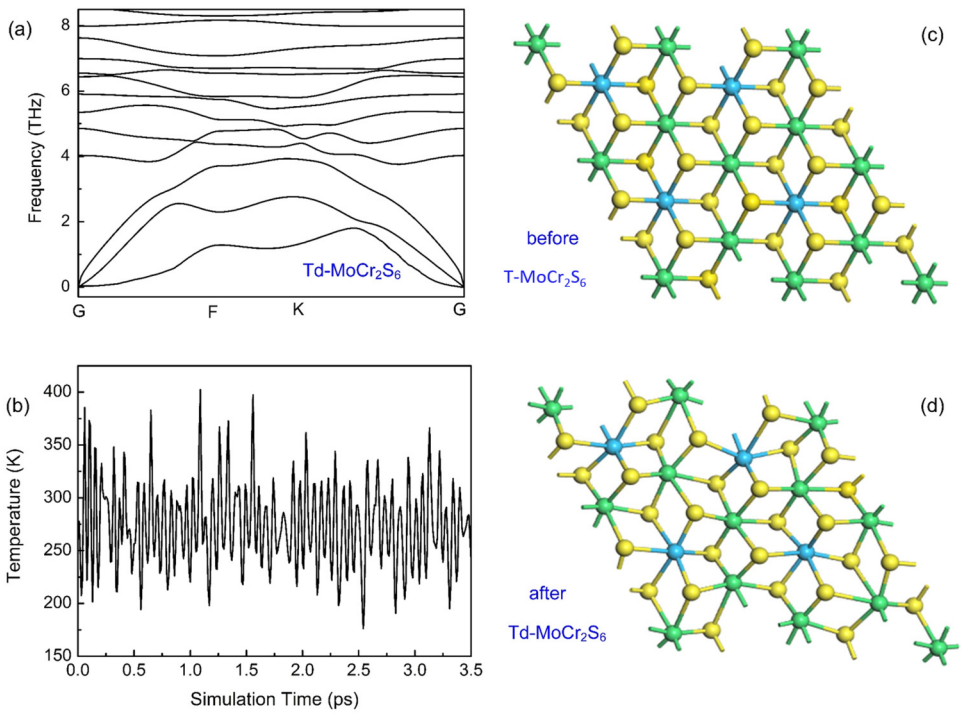

FIG. 3. (a) The calculated phonon dispersion of the Td-$MoCr_2S_6$ monolayer. (b) The fluctuation in temperature as a function of the molecular dynamic simulation step at 300 K for a (2 × 2 × 1) $MoCr_2S_6$ supercell. The results before (c) and after (d) simulation indicate that the symmetric T configuration can spontaneously transform into the distorted Td structure at 300 K.

calculated by $C_v = (\langle E^2\rangle - \langle E\rangle^2)/K_B T^2$, where E is the total energy of the system. The calculated magnetic anisotropy energy as a function of the external strain in Fig. S5 in the supplementary material discloses that the easy-axis flip is unlikely to occur in our proposed alloy.[25] Based on Monte Carlo simulations using the fitted parameters from HSE06 functional calculations, the spin structure factor $S(k)$ and specific heat C_v as functions of temperature are calculated as shown in Fig. 4(a). The Curie temperature is determined to be 145 K, which is higher than that of reported CrI_3.[13] We note that as a test, the Curie temperature of the CrI_3 monolayer is calculated to be 47 K using the same method, in agreement with the experimental value of 45 K.[13] In experiments, the structural deformation (smaller than 3%) can be easily acquired by growing a film on a substrate,[26–28] which provides a feasible strategy to enhance the magnetic coupling strength for room-temperature ferromagnetism. Indeed, the Curie temperature of $MoCr_2S_6$ can be enhanced by the biaxial tensile strain, as demonstrated in Fig. 4(b), which reaches at 300 K at approximately 1.8% biaxial tensile strain. If we take the thickness to be 5.8 Å, which is close to the interlayer space of bulk $MoCr_2S_6$, there still exists 20.1 $\mu C/cm^2$ ferroelectric polarization under approximately 1.8% strained conditions, which is comparable to those of recently reported 2D ferroelectric SnSe,[10] $BaTiO_3$ bulk,[29] phosphorene,[11] and $(CrBr_3)_2Li$.[3] Remarkably, a room-temperature multiferroicity is thus predicted in our proposed 2D $MoCr_2S_6$ monolayer.

The bandgap as a function of the tensile strain in Fig. 4(c) shows that tensile deformation keeps the system as a semiconductor with an increased gap. The projected density of states (PDOS) of the $MoCr_2S_6$ monolayer with 0.0% and 3.0% tensile strain are shown in Fig. 4(d) for comparison, whose bandgap is approximately 0.32 eV (0.0%) and 0.51 eV (3.0%), respectively. In addition, the spin splitting of PDOS in conduction band (marked by e_g orbitals) results in a typical magnetic semiconducting behavior, while the Cr cation possesses the half-filled t_{2g} configuration. The Curie temperature is mainly determined by magnetic exchange contribution between two Cr atoms. Based on the Goodenough–Kanamori rule,[30] the magnetic exchange between the half-filled orbitals (t_{2g}) is usually antiferromagnetic [see Fig. 4(e)]. Therefore, to realize the ferromagnetic exchange between Cr–Cr, the unfilled orbitals (e_g) must be taken into consideration, which are higher in energy than t_{2g} orbitals. The magnetic exchange interaction between half-filled t_{2g} orbitals and unfilled e_g orbitals is responsible for the ferromagnetic appearance. With the external tensile strain applied, the empty e_g levels move farther away from the occupied t_{2g} orbitals [Fig. 4(f)], which modifies the ferromagnetic exchange between Cr–Cr atoms. As a result, the effective ferromagnetic exchange strength is enhanced by the tensile deformation as shown in Fig. 5(a), in which the first-nearest magnetic coupling strength (J_1) plays a decisive role. In addition, Fig. 5(b) shows that the magnetic moment per Cr atom is slightly increased as an external strain. The robust ferromagnetic ordering due to the increased magnetic exchange interaction and enlarged magnetic moment demonstrates that applying tensile deformation can effectively increase the Curie temperature for ferromagnetism, while keeping ferroelectricity simultaneously.

To explain further why the T-$MoCr_2S_6$ monolayer prefers the Td configuration, the orbital-resolved band structures for T and Td phase are calculated and compared in Figs. 6(a) and 6(c),

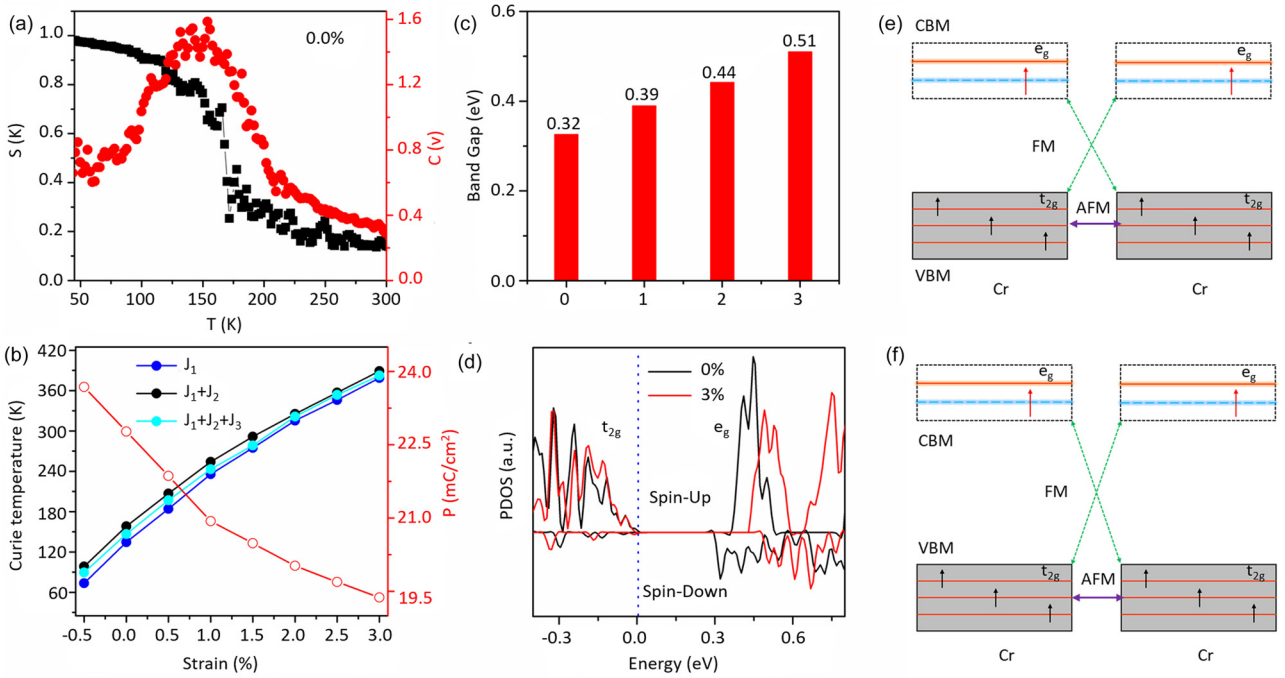

FIG. 4. (a) Simulated spin structure factor $S(k)$ and specific heat C_v as a function of temperature. (b) The Curie temperature including different magnetic coupling strengths and ferroelectric polarizations as a function of tensile strain. (c) The bandgap of the Td-$MoCr_2S_6$ monolayer with different tensile strains. (d) Projected density of states in the Td-$MoCr_2S_6$ monolayer under 0% and 3% tensile strain. The corresponding sketch of Cr orbitals and magnetic exchange in the Td-$MoCr_2S_6$ system without (e) and with tensile strain (f).

respectively. In the T-$MoCr_2S_6$ monolayer with a metallic feature, the d_{x2-y2} and d_{xz} orbitals of Mo atom cross together; meanwhile, the p_x and p_y orbitals of S3 and S5 sulfur atom [see labeling in Fig. 1(b)] are degenerate. In this case, the bond lengths of S3–Mo (2.414 Å) and S5–Mo (2.413 Å) are equal, and electrons prefer to occupy the bonding state formed through the hybridization between Mo-d_{x2-y2}, Mo-d_{xz} and S3-p_x, S5-p_y orbitals [see Fig. 6(b)]. Differently in the semiconducting Td phase, through Jahn–Teller distortion,[3] the Mo–S3 bond is compressed to 2.285 Å while the Mo–S5 bond is stretched to 2.638 Å [see Fig. 1(b)], leading to an unequal split of S3-p_x and S5-p_y states. It is known that the d orbitals of Mo atom are highly localized, which prohibits the hybridization between the lower S5-p_y orbital and the higher Mo-d_{xz} orbital [Fig. 6(d)]. Then, the electronic state composed of Mo-d_{x2-y2} and S3-p_x orbital prefers to be occupied (the bond orbital population is 0.55), while the hybridization between S3-p_x and S5-p_y is weakened (the bond orbital population is 0.16). The gain in electronic energy is mainly determined by the degree of the splitting between S3-p_x and S5-p_y

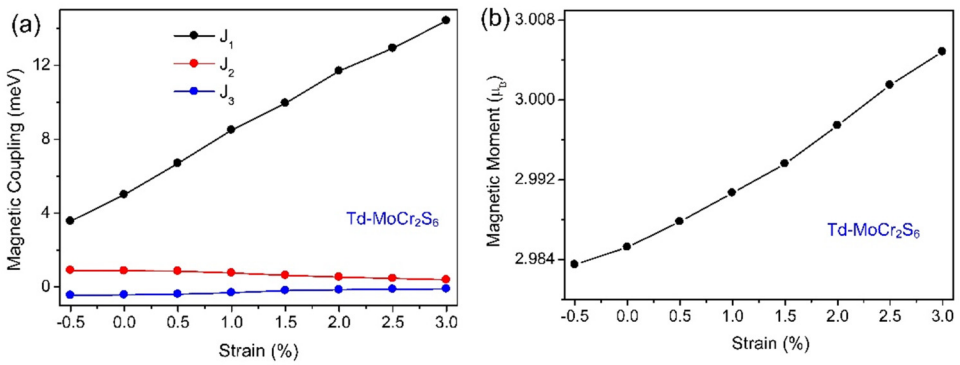

FIG. 5. (a) The magnetic coupling strength of the Td-$MoCr_2S_6$ monolayer under different tensile strains. (b) The magnetic moment per magnetic cation under different tensile strains.

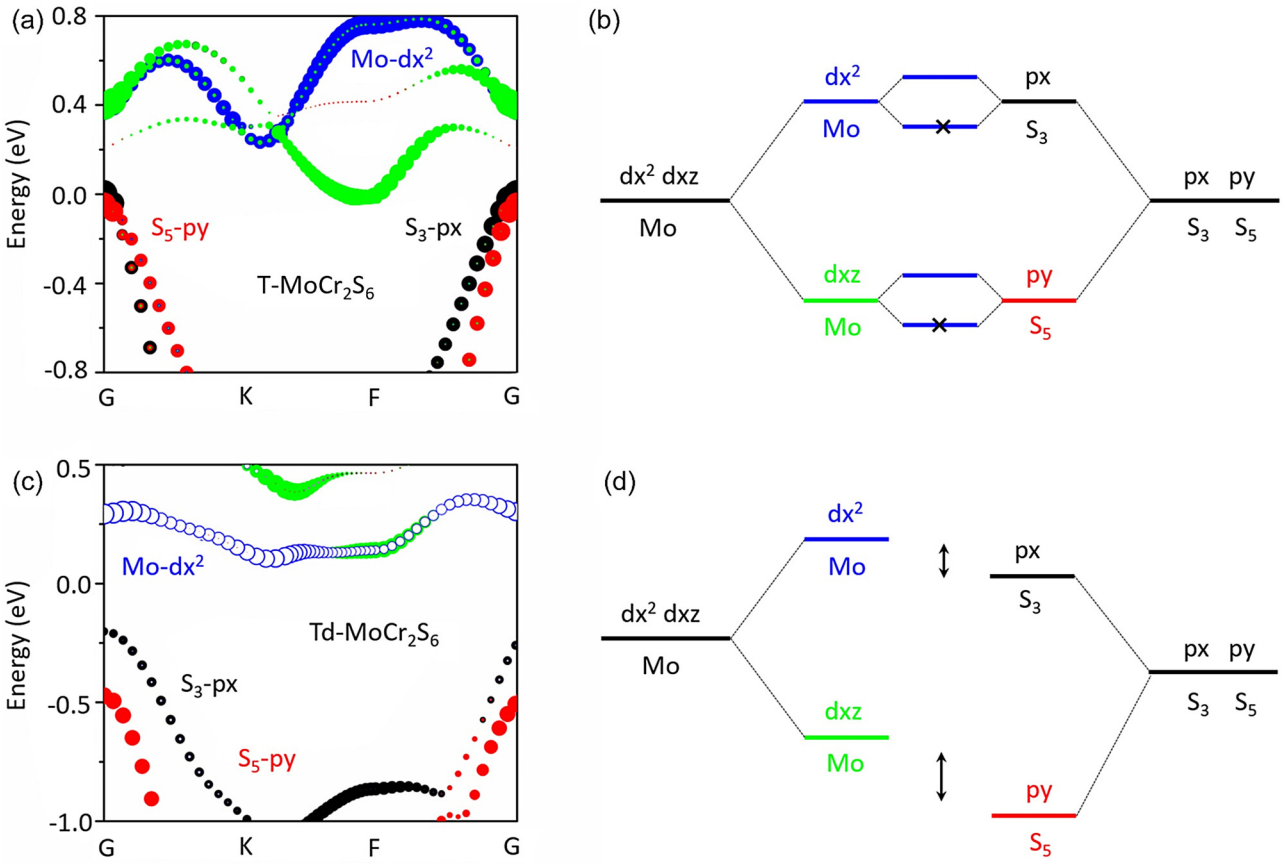

FIG. 6. The orbital-resolved band structure in T-$MoCr_2S_6$ (a) and Td-$MoCr_2S_6$ (c) monolayer. The evolution of electronic states for T-$MoCr_2S_6$ (b) and Td-$MoCr_2S_6$ (d).

orbitals. From Figs. 6(a) and 6(c), we see that the splitting of S3-p_x and S5-p_y orbitals in the Td structure (approximately 0.28 eV in energy) is much larger than that in the T structure (approximately 0.05 eV in energy), which again explains why asymmetric distortion is favored in this system. Thus, the Jahn–Teller-type metal-to-semiconductor transition from T to Td structure is responsible for the ferroelectric emergence.

IV. CONCLUSION

In conclusion, through a series of structural screening, a room-temperature 2D multiferroicity has been predicted in the $MoCr_2S_6$ monolayer under the external tensile strain. In this system, the ferroelectricity originates from asymmetric distortion of two neighboring Mo–S bonds via Mo atom displacement, accompanied by a spontaneous metal-to-semiconductor transition. Additionally, the magnetic exchange between two nearest-neighbor Cr atoms ensures a stable ferromagnetic ordering. The proposed approach can be generally applicable to obtain room-temperature ferroelectricity and ferromagnetism in other 2D alloys and be useful for designing multifunctional devices.

SUPPLEMENTARY MATERIAL

See the supplementary material for details of the calculated lattice constant with different U values and the magnetic anisotropy energy as a function of the tensile strain.

ACKNOWLEDGMENTS

This work was supported by the National Basic Research Program of China under Grant No. 2018YFA0306004, the Natural Science Foundation of Jiangsu Province (No. BK20171332), and the Fundamental Research Funds for the Central Universities (No. 0204-14380083). K.-H.J. and F.L. were supported by U.S. DOE-BES (No. DE-FG02-04ER46148).

REFERENCES

[1]W. Han, R. K. Kawakami, M. Gmitra, and J. Fabian, Nat. Nanotechnol. **9**, 794 (2014).
[2]Y. Zhao, L. Lin, Q. Zhou, Y. Li, S. Yuan, Q. Chen, S. Dong, and J. Wang, Nano Lett. **18**, 2943 (2018).
[3]C. Huang, Y. Du, H. Wu, H. Xiang, K. Deng, and E. Kan, Phys. Rev. Lett. **120**, 147601 (2018).

[4]J. Qi, H. Wang, X. Chen, and X. Qian, Appl. Phys. Lett. **113**, 043102 (2018).
[5]M. Wang, X. Sui, Y. Wang, Y.-H. Juan, Y. Lvu, H. Peng, T. Huang, S. Shen, C. Guo, J. Zhang *et al.*, Adv. Mater. **31**, 1900458 (2019).
[6]N. A. Hill, J. Phys. Chem. B **104**, 6694 (2000).
[7]C. Gong, E. M. Kim, Y. Wang, G. Lee, and X. Zhang, Nat. Commun. **10**, 2657 (2019).
[8]S. N. Shirodkar and U. V. Waghmare, Phys. Rev. Lett. **112**, 157601 (2014).
[9]E. Kan, F. Wu, K. Deng, and W. Tang, Appl. Phys. Lett. **103**, 193103 (2013).
[10]R. Fei, W. Kang, and L. Yang, Phys. Rev. Lett. **117**, 097601 (2016).
[11]M. Wu and X. C. Zeng, Nano Lett. **16**, 3236 (2016).
[12]H. Wang and X. F. Qian, 2D Mater. **4**, 015042 (2017).
[13]B. Huang, G. Clark, E. Navarro-Moratalla, D. R. Klein, R. Chen, K. L. Seyler, D. Zhong, E. Schmidgall, M. A. McGuire, D. H. Cobden *et al.*, Nature **546**, 270 (2017).
[14]C. Gong, L. Li, Z. Li, H. Ji, A. Stern, Y. Xia, T. Cao, W. Bao, C. Wang, Y. Wang *et al.*, Nature **546**, 265 (2017).
[15]G. Kresse and J. Hafner, Phys. Rev. B **47**, 558 (1993).
[16]J. P. Perdew, K. Burke, and M. Ernzerhof, Phys. Rev. Lett. **77**, 3865 (1996).
[17]S. L. Dudarev, G. A. Botton, S. Y. Savrasov, C. J. Humphreys, and A. P. Sutton, Phys. Rev. B **57**, 1505 (1998).
[18]R. D. King-Smith and D. Vanderbilt, Phys. Rev. B **47**, 1651 (1993).
[19]C. Xu, Y. Yang, S. Wang, S. Y. Wang, W. Duan, B. Gu, and L. Bellaiche, Phys. Rev. B **89**, 205122 (2014).
[20]H. Tang, C. Xu, M. Li, S. Wang, B.-L. Gu, and W. Duan, J. Phys. Condens. Matter **28**, 126002 (2016).
[21]D.-H. Seo, J. Lee, A. Urban, R. Malik, S. Y. Kang, and G. Ceder, Nat. Chem. **8**, 692 (2016).
[22]Z.-F. Huang, J. Song, Y. Du, S. Xi, S. Dou, J. M. V. Nsanzimana, C. Wang, Z. J. Xu, and X. Wang, Nat. Energy **4**, 329 (2019).
[23]C. Wang, X. Zhou, Y. Pan, J. Qiao, X. Kong, C.-C. Kaun, and W. Jin, Phys. Rev. B **97**, 245409 (2018).
[24]N. Metropolis and S. Ulam, J. Am. Stat. Assoc. **44**, 335 (1949).
[25]C. Xu, J. Feng, H. Xiang, and L. Bellaiche, NPJ Comput. Mater. **4**, 57 (2018).
[26]M. Huang, H. Yan, T. F. Heinz, and J. Hone, Nano Lett. **10**, 4074 (2010).
[27]H. Li, C. Tsai, A. L. Koh, L. Cai, A. W. Contryman, A. H. Fragapane, J. Zhao, H. S. Han, H. C. Manoharan, F. Abild-Pedersen *et al.*, Nat. Mater. **15**, 48 (2016).
[28]C. Zhang, M.-Y. Li, J. Tersoff, Y. Han, Y. Su, L.-J. Li, D. A. Muller, and C.-K. Shih, Nat. Nanotechnol. **13**, 152 (2018).
[29]K. J. Choi, M. Biegalski, Y. L. Li, A. Sharan, J. Schubert, R. Uecker, P. Reiche, Y. B. Chen, X. Q. Pan, V. Gopalan *et al.*, Science **306**, 1005 (2004).
[30]J. Goodenough, Scholarpedia **3**, 7382 (2008).